ISTITUTO NAZIONALE DI RICERCA METROLOGICA
Repository Istituzionale

Phase-Noise and Amplitude-Noise Measurement of DACs and DDSs

(Article begins on next page)

28 April 2024

Phase-Noise and Amplitude-Noise Measurement of DACs and DDSs

Claudio E. Calosso, A. Carolina Cárdenas Olaya, and Enrico Rubiola

Abstract— This article proposes a method for the measurement of phase noise (PN, or PM noise) and amplitude noise (AN, or AM noise) of digital-to-analog converters (DACs) and direct digital synthesizers (DDSs) based on the modulation-index amplification. The carrier is first reduced by a controlled amount (30–40 dB) by adding a reference signal of nearly equal amplitude and opposite in phase. Then, residual carrier and noise sidebands are amplified and sent to a conventional PN analyzer. The main virtues of our method are: 1) the noise specs of the PN analyzer are relaxed by a factor equal to the carrier suppression ratio and 2) the capability to measure the AN using a PN analyzer with no need for the analyzer to feature AN measurement. An obvious variant enables AN and PN measurements using an AN analyzer with no PN measurement capability. Such an instrument is extremely simple and easy to implement with a power-detector diode followed by an FFT analyzer. Unlike the classical bridge (interferometric) method, there is no need for external line stretcher and variable attenuators because phase and amplitude controls are implemented in the device under test. In one case (AD9144), we could measure the noise over 10 decades of frequency. The flicker noise matches the exact $1/f$ law with a maximum discrepancy of ± 1 dB over 7.5 decades. Due to the simplicity, reliability, and low background noise, this method has the potential to become the standard method for the AN and PN measurements of DACs and DDSs.

Index Terms— Analog-digital integrated circuits, integrated circuit noise, noise measurement, phase noise, signal synthesis.

I. Introduction and State of the Art

IN VIRTUALLY all domains of technology, RF electronics is going digital via dedicated hardware, FPGA processing, and software-defined radio techniques, and analog-to-digital converters (ADCs) and digital-to-analog converters (DACs) are ubiquitous. This major trend is obviously driven by big

C. E. Calosso and A. C. Cárdenas Olaya are with the Division of Quantum Metrology and Nanotechnology, Istituto Nazionale di Ricerca Metrologica (INRiM), 10135 Turin, Italy (e-mail: c.calosso@inrim.it).

E. Rubiola is with the Department of Time and Frequency, FEM-TOST Institute, Université de Bourgogne and Franche-Comté (UBFC), CNRS, 25000 Besançon, France, and also with the Division of Quantum Metrology and Nanotechnology, Istituto Nazionale di Ricerca Metrologica (INRiM), 10135 Turin, Italy (e-mail: rubiola@femto-st.fr).

telecom companies for mass consumer products and infrastructure equipment. While basic principles of conversion are rather mature [1, ch. 1–3], all the development is confidential. The technical information about converters and digital frequency synthesis is now in magazines [2]–[7] and books [8], [9], [10], [11, ch. 3], [12], [13, ch. 9–11].

Converters are available from leading manufacturers (chiefly, Analog Devices, Linear Technology, and Texas Instruments) with several GHz clock speed, 12–16 b (BUS), and up to 12–13 equivalent number of bits (ENOB). High-speed ADCs are generally more complex than DACs and have an inferior tradeoff between the ENOB and the maximum clock frequency. The reason is that most ADC architectures (SAR, pipelined, and subranging flash) employ a DAC.

Our interest is oriented toward scientific applications, where the demand for high-purity RF signals is ever-growing. The relevant parameters are low PM and AM noises, high stability, frequency agility, and programmable amplitude and phase. We have in mind, general-purpose instruments, atomic–molecular–optics physics and atomic clocks [14]–[16], long-distance synchronization via fiber links [17]–[19], real-time phase measurements [20], particle accelerators [21], and so on.

In this context, we focus on the AM and PM noises of DACs and direct digital synthesizers (DDSs). Interestingly, modern high-speed telecom-oriented DACs have an internal numerically controlled oscillator (NCO), which makes the DAC very similar to the DDS. If not, the NCO can be implemented in FPGA, transferring the data to the DAC via the JESD204B interface. Thus, we refer to the term DAC as a placeholder for both DAC and DDS.

Going through numerous data sheets, we see that manufacturers are most concerned with SFDR, SINAD, THD and ENOB, and leakage from/to adjacent channels (see for example [1, ch. 2] for the definition of these terms). By contrast, phase noise (PN) is generally documented only as a typical plot of $\mathscr{L}(f)$ in a reference condition, starting from $f = 10$ Hz. It is often difficult to distinguish the device's PN from the contribution of the reference oscillator and of the PN analyzer. The literature says quite little about PN in DACs and about how it is measured. Delos and Liner [22] provide some useful tips based on the general RF/microwave methods for PM noise measurement. The AM noise is neither seen in the data sheets nor in the technical literature.
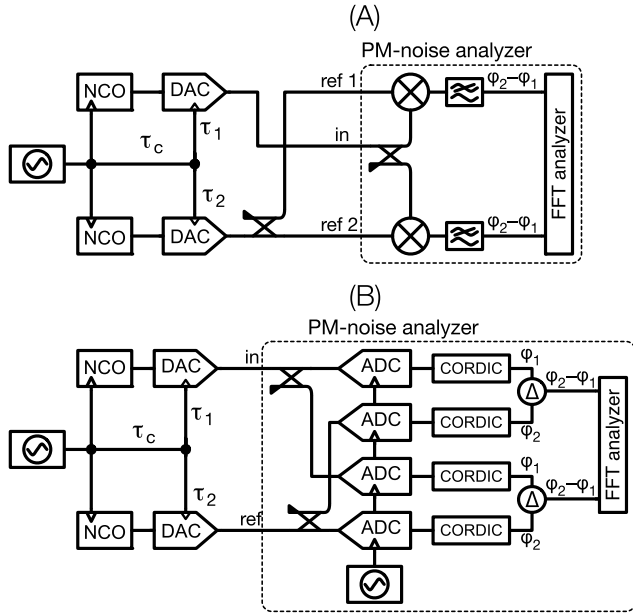
We describe the noise as the power spectral density (PSD) of the random phase $\varphi(t)$ and fractional amplitude $\alpha(t)$,

Fig. 1.   Traditional phase-noise analyzers used for the measurement of DACs. The PM noise spectrum results from the contribution of the two DACs. The FFT analyzer measures the average cross PSD of the two inputs "$\varphi_2 - \varphi_1$," and thus, it rejects the noise components present only at one input. Notice that the single-DAC clock fluctuations τ_1 and τ_2 (included in φ_1 and φ_2) are detected, while the common-mode clock fluctuation τ_C is rejected because it cancels in $\varphi_2 - \varphi_1$. (a) Saturated mixer. (b) Fully digital.

denoted with $S_\varphi(f)$ and $S_\alpha(f)$ as a function of the Fourier frequency f. Note that the more popular quantity $\mathscr{L}(f) \triangleq (1/2)S_\varphi(f)$ is defined only for PN. We use the polynomial law $S_\varphi(f) = \mathsf{b}_0 + \mathsf{b}_{-1}/f + \cdots$ and $S_\alpha(f) = \mathsf{h}_0 + \mathsf{h}_{-1}/f + \cdots$ truncated after the flicker term $1/f$, as appropriated for two-port components. The reader may refer to [23]–[25] for an introduction to PM noise and to [26] for AM noise.

Measuring some DDSs with various methods, we observed that the white noise coefficient b_0 can be of -165 dBrad^2/Hz. The flicker coefficient b_{-1} can be of -135 dBrad^2 at 10-MHz output frequency and -110 dBrad^2 at 100–150-MHz output. We published only a part of this at a conference [27]. Anyway, these numerical values define the minimum requirement for the background noise.

Fig. 1 shows the direct measurement of the DAC noise with commercial PN analyzers. All such instruments achieve reduced background noise by correlating and averaging the output of two channels.

The classical PN analyzer is based on a saturated mixer close to the quadrature condition, which converts the input phase into a voltage. In our case, the quadrature condition can be set numerically, provided the symmetry is sufficient to set the two channels at once. A problem is the high saturation power of the mixer (7–15 dBm) compared to the low output power of the DACs (≈ 0 dBm). The power splitters introduce additional 3-dB intrinsic loss. The signal can be amplified, but the amplifiers add complexity and noise. A three-DAC version shown in Fig. 1(a) is also possible, which measures the noise of one DAC and rejects the noise of the other two [22, Fig. 4(b)].
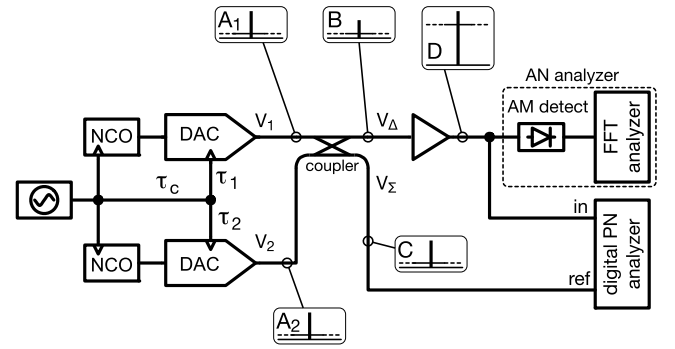
Fig. 2.   Measurement method. The rounded rectangles show the relevant spectra in log scale.

Conversely, the fully digital analyzer is based on the direct AD conversion of the input signal [28]. The benefit is obvious in that the instrument accepts different frequencies at the "in" and "ref" inputs, and of course, there is no phase adjustment. At the time of writing, such test sets are available from only two brands: Microsemi (formerly Symmetricom) [29] and Jackson Labs [30, scheduled mid/late 2019]. The Rohde Schwarz FSWP [31], [32] is a digital instrument with downconversion from microwaves, but it is still unclear to us whether the "ref" input is suitable to our purposes.
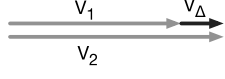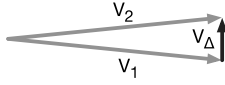
II. Principles and Method

Our method relies on the modulation-index amplification by a factor $1/\eta \gg 1$, introduced later. After amplification, the AM and PM noises are so high that the correlation is not necessary. This solves two problems at once. First, the correlation instruments rely on the hypothesis that the two channels are statistical independent. This is sometimes untrue and hard to check. Gross errors are possible if the experimentalist does not have a deep understanding (see [33], [34]). The second problem is the measurement time, chiefly with the digital instruments because the noise of the DACs under test is often lower than that of the input ADCs. In fact, the noise rejection is proportional to $1/\sqrt{m}$, where m is the number of the FFTs averaged. This means 5 dB per factor of 10. Accordingly, if an FFT starting from 1 mHz takes 2000-s acquisition time, averaging over 100 spectra for 10-dB noise rejection takes a measurement time of 2 days and 7.5 h. A large m is often necessary with the correlation instruments to reject the single-channel noise and to smooth the spectrum. By contrast, our method does not rely on noise rejection by averaging. A comparatively smaller m is needed only for smoothing. An extensive treatise about the noise rejection and the spectrum smoothing is available in [35].

The scheme shown in Fig. 2 illustrates our method to measure the noise of two equal devices under test (DUT). The rectangles labeled A$_1$, A$_2$, B, C, and D show the spectrum in the critical points, in log scale. The two signals V_1 and V_2 are combined in the directional coupler so that almost all the carrier power goes at the Σ output, and a small power goes to the Δ output. However, the noise sidebands are equally split between the Σ and Δ outputs because these signals are not coherent (spectra B and C). Residual carrier and noise sidebands are amplified (spectrum D) and detected by the PN analyzer or by the amplitude noise (AN) analyzer.

Our method derives from an early idea for the PN measurement of microwave two-port devices [36]. In the original version, the reference carrier crosses the DUT, which contributes its own noise. The carrier is completely suppressed by subtracting a copy of the reference through a magic Tee (a waveguide directional coupler), and the DUT noise sidebands are downconverted to dc by synchronous detection. Microwave amplification of the noise sidebands was added later to boost the gain and to reduce the background noise [37]. The whole system is equivalent to a Wheatstone bridge powered by an ac signal (the microwave carrier), followed by a lock-in amplifier. The lowest background noise is achieved after adjusting the system for the maximum carrier rejection [38], [39]. By contrast, we leave a carefully controlled amount of carrier, as proposed in [40] for different purposes. There results a modulation-index amplification, with optional AM-to-PM and PM-to-AM conversions depending on the phase relationships. The presence of the residual carrier is essential in that it makes the signal suitable to the measurement with all-digital PN analyzers or with a simple AN analyzer implemented with a power-detector diode ($100–300 for a packaged and connectorized detector) and an FFT spectrum analyzer [26]. Due to the AM-to-PM and PM-to-AM conversion, a PN analyzer with no AN measurement capability enables the measurement of both AN and PN. Likewise, an AN analyzer with no PN measurement capability enables the same measurements. The modulation-index amplification relaxes the noise specs of the PN analyzer or of the AN analyzer, by the same factor. The RF gain (40–60 dB) is needed for the power to match the input range of the PN or AN analyzer.

The background white noise is due to the noise FkT of the amplifier, where F is the amplifier noise figure (1–2 dB, that is, 1.25–1.6) and $kT \approx 4 \times 10^{-21}$ W/Hz is the thermal energy at room temperature. Converted into PM noise, the background is $\mathbf{b}_0 = 2FkT/P$, where P is the carrier power at the directional-coupler input and the factor "2" accounts for the inherent 3-dB loss in the coupler. The background $1/f$ PM noise is that of the amplifier, divided by the carrier suppression ratio. This happens because the $1/f$ PN in components results from parametric upconversion of the near-dc noise [41].

A. Modulation-Index Amplification

The directional coupler in Fig. 2 delivers the output

$$V_\Delta = \frac{1}{\sqrt{2}}(V_2 - V_1) \tag{1}$$

where V_1 and V_2 are the output signals of the two converters and the factor $1/\sqrt{2}$ is due to energy conservation in the absence of loss. These signals have random fractional amplitudes $\alpha_1(t)$ and $\alpha_2(t)$ and random phases $\varphi_1(t)$ and $\varphi_2(t)$. We assume that $|\alpha_1| \ll 1$, $|\alpha_2| \ll 1$, $|\varphi_1| \ll 1$, and $|\varphi_2| \ll 1$; hence, $e^{\alpha+j\varphi} \simeq 1 + \alpha + j\varphi$.

For our purposes, it is convenient to set V_1 and V_2 close to the nominal amplitude V_0 but for a small difference in amplitude (β_1 and β_2) and phase (γ_1 and γ_2) so that

$$V_1 = V_0(1 - \beta_1)e^{-i\gamma_1}e^{\alpha_1+j\varphi_1} \tag{2}$$
$$V_2 = V_0(1 + \beta_2)e^{+i\gamma_2}e^{\alpha_2+j\varphi_2}. \tag{3}$$

Fig. 3. Interplay between signals at the output of the directional coupler. In the actual RF circuit, all signals are scaled up by a factor $V_0/\sqrt{2}$, omitted for graphical clarity.

Fig. 3 shows these signals and how they combine to form V_Δ. The latter can be written as

$$V_\Delta = \eta \frac{V_0}{\sqrt{2}} e^{j\theta} e^{\epsilon+j\psi} \tag{4}$$

where η and θ describe the static amplitude and phase of the carrier seen at the coupler output and $\epsilon(t)$ and $\psi(t)$ describe the amplitude and phase modulations. We will show that $1/\eta$ is the modulation-index amplification. The quantity η has to satisfy $|\epsilon + j\psi| \ll \eta \ll 1$. First, $\eta \ll 1$ is necessary for the amplification to be useful. Second, $\eta \gg |\epsilon + j\psi|$ is needed to prevent V_Δ from sweeping 0. If this happens, AM and PM are no longer defined. Because AM and PM noise are small, these conditions allow a large range for η.

The desired amount of residual carrier is obtained by setting β_1, β_2, γ_1, and γ_2 to appropriate values. Notice that β_1 and β_2, and likewise γ_1 and γ_2, are not equal in the general case, but they can be assumed equal for $\eta \ll 1$. Accordingly, it is useful to set $\beta_1 = \beta_2 = \beta/2$ and $\gamma_1 = \gamma_2 = \gamma/2$, which defines β and γ. By the inspection on Fig. 3, it holds that $\beta \ll 1$ and $\gamma \ll \theta$ for $\eta \ll 1$.

Combining (1)–(3) gives

$$V_\Delta = \frac{V_0}{\sqrt{2}} \left[\left(1 + \frac{\beta}{2} \right) e^{j\gamma/2} e^{\alpha_2+j\varphi_2} + \right.$$
$$\left. - \left(1 - \frac{\beta}{2} \right) e^{-j\gamma/2} e^{\alpha_1+j\varphi_1} \right]. \tag{5}$$

The AM and PM associated with V_Δ result from

$$\epsilon = \Re\left\{ \frac{\mathcal{S}}{\mathcal{C}} \right\} \quad \text{and} \quad \psi = \Im\left\{ \frac{\mathcal{S}}{\mathcal{C}} \right\} \tag{6}$$

where

$$\mathcal{S} = \frac{V_0}{\sqrt{2}} \left[\left(1 + \frac{\beta}{2} + j\frac{\gamma}{2} \right) (\alpha_2 + j\varphi_2) + \right.$$
$$\left. - \left(1 - \frac{\beta}{2} - j\frac{\gamma}{2} \right) (\alpha_1 + j\varphi_1) \right] \tag{7}$$

is the voltage swing of (5) and

$$\mathcal{C} = \eta \frac{V_0}{\sqrt{2}} e^{j\theta} \tag{8}$$

TABLE I
MEASUREMENT OPTIONS

Operation	PN-analyzer only	AN-analyzer only	Signal vectors
$\theta = 0$ AN and PN amplification	$S_\psi \simeq \dfrac{S_{\varphi 2} + S_{\varphi 1}}{\eta^2}$	$S_\epsilon \simeq \dfrac{S_{\alpha 2} + S_{\alpha 1}}{\eta^2}$	
$\theta = \pi/2$ AN-PN cross amplification	$S_\psi \simeq \dfrac{S_{\alpha 2} + S_{\alpha 1}}{\eta^2}$	$S_\epsilon \simeq \dfrac{S_{\varphi 2} + S_{\varphi 1}}{\eta^2}$	

is the carrier. Recalling that $\beta \ll 1$ and $\gamma \ll \theta$ for $\eta \ll 1$, (6) can be elegantly rewritten as

$$\begin{bmatrix} \epsilon \\ \psi \end{bmatrix} = \frac{1}{\eta} \begin{bmatrix} \cos\theta & \sin\theta \\ -\sin\theta & \cos\theta \end{bmatrix} \begin{bmatrix} \alpha_2 - \alpha_1 \\ \varphi_2 - \varphi_1 \end{bmatrix}. \tag{9}$$

The matrix represents a rotation by $-\theta$ that comes from the fact that I and Q (in-phase and quadrature voltage swing) are projected on V_Δ. The term $1/\eta$ means that I and Q are now referred to a carrier of amplitude $\eta \ll 1$, which results in proportionally larger fractional amplitude or phase swing. Equation (9) emphasizes the following two key concepts.

1) The modulation index is amplified by a factor $1/\eta$.
2) The rotation enables to preserve the character of AM and PM ($\theta = 0$), to interchange AM and PM ($\theta = \pi/2$), or to take any combination of AM and PM.

Replacing ϵ and ψ with their spectra, (9) becomes

$$\begin{bmatrix} S_\epsilon \\ S_\psi \end{bmatrix} = \frac{1}{\eta^2} \begin{bmatrix} \cos^2\theta & \sin^2\theta \\ \sin^2\theta & \cos^2\theta \end{bmatrix} \begin{bmatrix} S_{\alpha 2} + S_{\alpha 1} \\ S_{\varphi 2} + S_{\varphi 1} \end{bmatrix} \tag{10}$$

which enables the measurement options listed in Table I.

It is important to remember that (10) relies on the assumption that the noise of the two converters is uncorrelated because the system is insensitive to common-mode noise. This is clear with the PM noise: the common-mode time fluctuation τ_c is rejected, which includes the clock (see Fig. 2). By contrast, correlation in the AM noise is more subtle because it originates from the power supply and from the voltage reference. Insufficient power supply rejection ratio (PSRR) may result in correlated noise, and multiple DACs in a chip may share the reference.

B. Exact Analysis

We evaluate the errors due to the hypothesis that $\eta \ll 1$. With reference to Fig. 3, β_1 and β_2, and likewise γ_1 and γ_2, are not equal in the general case. Combining (1)–(3) gives

$$V_\Delta = \frac{V_0}{\sqrt{2}} \left[(1+\beta_2) e^{j\gamma_2} e^{\alpha_2 + j\varphi_2} - (1-\beta_1) e^{-j\gamma_1} e^{\alpha_1 + j\varphi_1} \right]. \tag{11}$$

In low-noise conditions, the associated voltage swing is

$$\mathcal{S} = \frac{V_0}{\sqrt{2}} \left[(1+\beta_2) e^{j\gamma_2} (\alpha_2 + j\varphi_2) - (1-\beta_1) e^{-j\gamma_1} (\alpha_1 + j\varphi_1) \right]. \tag{12}$$

Putting the above-mentioned expression of $\mathcal{S}$ in (6) gives

$$\epsilon = \frac{1+\beta_2}{\eta} \left[\alpha_2 \cos(\theta - \gamma_2) + \varphi_2 \sin(\theta - \gamma_2) \right] - \frac{1-\beta_1}{\eta} \left[\alpha_1 \cos(\theta + \gamma_1) + \varphi_1 \sin(\theta + \gamma_1) \right] \tag{13}$$

$$\psi = \frac{1+\beta_2}{\eta} \left[-\alpha_2 \cos(\theta - \gamma_2) + \varphi_2 \sin(\theta - \gamma_2) \right] - \frac{1-\beta_1}{\eta} \left[-\alpha_1 \cos(\theta + \gamma_1) + \varphi_1 \sin(\theta + \gamma_1) \right]. \tag{14}$$

Using the matrix expression of the above-mentioned expression for the spectra of uncorrelated DACs, similar to (10), yields

$$\begin{bmatrix} S_\epsilon \\ S_\psi \end{bmatrix} = \frac{(1+\beta_2)^2}{\eta^2} [A_2] \begin{bmatrix} S_{\alpha 2} \\ S_{\varphi 2} \end{bmatrix} + \frac{(1-\beta_1)^2}{\eta^2} [A_1] \begin{bmatrix} S_{\alpha 1} \\ S_{\varphi 1} \end{bmatrix} \tag{15}$$

with

$$[A_2] = \begin{bmatrix} \cos^2(\theta - \gamma_2) & \sin^2(\theta - \gamma_2) \\ \sin^2(\theta - \gamma_2) & \cos^2(\theta - \gamma_2) \end{bmatrix} \tag{16}$$

$$[A_1] = \begin{bmatrix} \cos^2(\theta + \gamma_1) & \sin^2(\theta + \gamma_1) \\ \sin^2(\theta + \gamma_1) & \cos^2(\theta + \gamma_1) \end{bmatrix}. \tag{17}$$

We introduce the approximation that $S_{\alpha 1} \simeq S_{\alpha 2}$ and $S_{\varphi 1} \simeq S_{\varphi 2}$, based on the fact that the two DACs are nominally equal. Thus, it makes sense to approximate (15) as

$$\begin{bmatrix} S_\epsilon \\ S_\psi \end{bmatrix} = \frac{1}{\eta^2} [A] \begin{bmatrix} S_{\alpha 2} + S_{\alpha 1} \\ S_{\varphi 2} + S_{\varphi 1} \end{bmatrix} \tag{18}$$

averaging the two matrices

$$[A] = \frac{1}{2} \left\{ (1+\beta_2)^2 [A_2] + (1-\beta_1)^2 [A_1] \right\}. \tag{19}$$

From the geometrical properties shown in Fig. 4, the Pythagoras theorem gives

$$(1+\beta_2)^2 = \left(1 + \frac{\eta}{2}\cos\theta \right)^2 + \left(\frac{\eta}{2}\sin\theta \right)^2 \tag{20}$$

$$(1-\beta_1)^2 = \left(1 - \frac{\eta}{2}\cos\theta \right)^2 + \left(\frac{\eta}{2}\sin\theta \right)^2 \tag{21}$$

$$\gamma_2 = \arctan\left(\frac{\frac{\eta}{2}\sin\theta}{1 + \frac{\eta}{2}\cos\theta} \right) \tag{22}$$

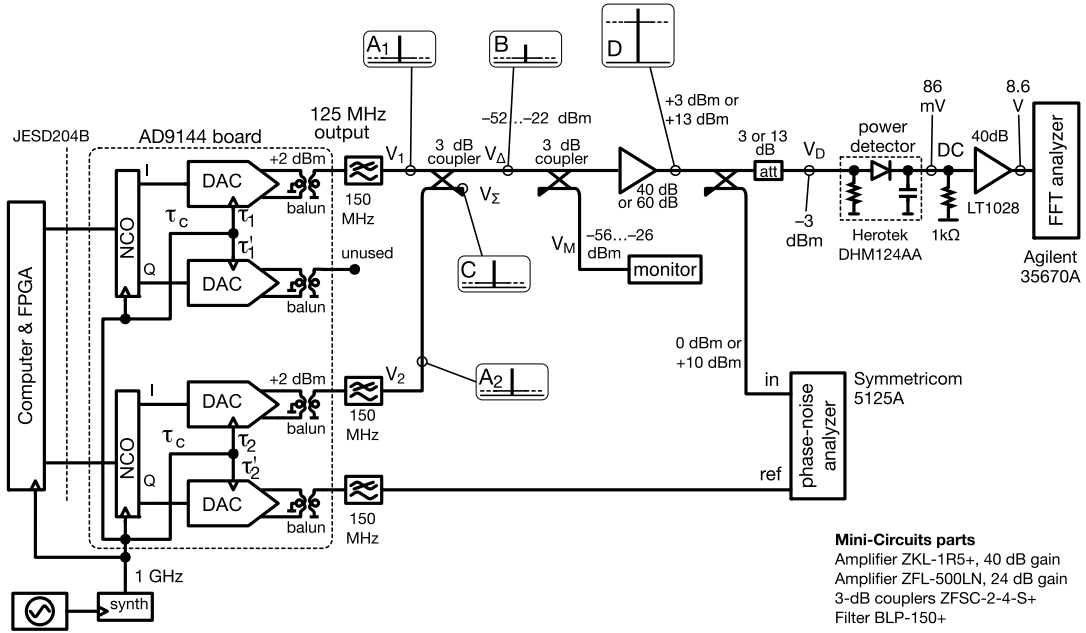$$\gamma_1 = \arctan\left(\frac{\frac{\eta}{2}\sin\theta}{1 - \frac{\eta}{2}\cos\theta} \right). \tag{23}$$

Fig. 4. Geometrical properties from Fig. 3.

Putting (20)–(23) into (15) and expanding (18), we get a general expression for $[A]$. The derivation of $[A]$ and the subsequent manipulations are done with a symbolic math app (Wolfram Mathematica). Since the full expression of $[A]$ is too complex and hard to read, we omit it and we discuss three relevant cases. The first case is

$$\lim_{\eta \to 0} [A] = \begin{bmatrix} \cos^2(\theta) & \sin^2(\theta) \\ \sin^2(\theta) & \cos^2(\theta) \end{bmatrix} \quad (24)$$

which is equivalent to (10) and validates on rigorous basis the simplified approach of Section II-A.

The second case is the accuracy of (18) for $\theta = 0$, still under the assumption that the noise of the two DACs is equal. For this purpose, we allow a small angle error ζ, and we expand (15) in series truncated to the second order of η and ζ. For $\theta = 0$, replacing $\theta \to \zeta$ gives

$$[A] = \begin{bmatrix} 1 + \eta^2/4 - \zeta^2 & \zeta^2 \\ \zeta^2 & 1 + \eta^2/4 - \zeta^2 \end{bmatrix}. \quad (25)$$

The third case is the accuracy of (18) for $\theta = \pi/2$, analyzed in the same way as before but for $\theta = \pi/2 + \zeta$. Hence

$$[A] = \begin{bmatrix} \zeta^2 + \eta^2/4 & 1 - \zeta^2 \\ 1 - \zeta^2 & \zeta^2 + \eta^2/4 \end{bmatrix}. \quad (26)$$

The finite gain results in small errors, negligible in most practical cases. For example, $1/\eta^2 = 100$ (20 dB) results in 1.1×10^{-2} dB error in (25) and in -26-dB coupling between AM and PM in (26). Of course, the gain must be well calibrated because of the $1/\eta^2$ factor in (15). The angle error deserves more attention. For example, $\zeta = 0.1$ (5.7°) results in -4.4×10^{-2} dB error and -20-dB coupling between AM and PM in both (25) and (26). The PM noise is generally dominant because of the jitter in the clock distribution and may pollute the AM noise measurement.

III. EXPERIMENTS

We measured the two channels of an AD9144 with the scheme shown in Fig. 5. The four channels of the AD9144 go in pairs with two NCOs. The two channels that we measure can be considered as separated devices but for small crosstalk and the small jitter τ_c in the common-mode clock path. The AD9144 is driven by a Z-Board ZC706 via the JESD204B interface. The ZC706 is a computer based on a Zynq-7000

with flash memory, DDR3 memory, Ethernet, USB, SD card slot, HDMI video, and SPI and FMC connectors for daughterboards. It runs Linaro Linux. In turn, the Zynq-7000 is a System on Chip (SoC), which is basically a microprocessor and an FPGA on the same chip.

The AD9144 is actually an AD9144-FMC-EBZ card [42], which contains the AD9144 chip, the AD9516-0 clock generator, the output baluns, and the auxiliary functions. This card is plugged into the FMC connector of the Z-Board and delivers $+2$-dBm power on the 50-Ω load on each output (SMA connector). The speed of the JESDB204B sufficient to set instantaneous phase and amplitude, but in our case such, speed is needed only for the amplitude because phase and frequency are static parameters, set only once.

Most of the tests were done in Turin with the exact scheme shown in Fig. 5 and with $1/\eta$ from 20 to 49 dB. Table II shows the operating parameters. However, preliminary tests were done in Besançon using a slightly different configuration and no power detector. The output V_Σ was used as the carrier-rejection monitor and, later in the experiment, as the reference of the PN analyzer. This saves one coupler on the RF path and results in 3-dB lower background noise.

The AD9144 data sheet does not indicate the ENOB. Instead, it gives the typical white noise of -162 dBm/Hz ($N = 6.3 \times 10^{-20}$ W/Hz) with 150 MHz single-tone output, full amplitude, and 983.04-MHz sampling frequency. These conditions are quite similar to ours. The white AN follows from $S_\alpha = N/P$, where P is the output power. The PN follows from $S_\varphi = N/P + J$, where J is the additional contribution of the clock jitter, unknown here and not impacting on the AN. From the specs, we expect $S_\alpha = -164$ dB/Hz with $+2$-dBm output power and $S_\alpha = -161$ dB/Hz for the noise of two channels.

Accounting for 7-dB loss from the DAC output to the input of the RF amplifier (low-pass filter and two 3-dB couplers) and adding the independent contribution of two DACs, the expected noise is of -166 dBm/Hz at the input of the RF amplifier. This value is 8 dB higher than the thermal noise at room temperature (-174 dBm/Hz). Allowing a noise figure of 2 dB, the amplifier contributes $+1$ dB to the noise limit.

The AN measurement is performed with a single-channel system (power detector, amplifier, and FFT analyzer). The Schottky diode detector has two modes of operation. The true power detection ($V_{out} \propto P_{in}$) relies on the linearization of the exponential $V(I)$ characteristics of the diode, which is valid for the peak voltage $V_{in} \lesssim V_T = kT/q$. This corresponds to approximately -20-dBm input power on 50 Ω. At a higher power, peak detection occurs ($V_{out} \propto V_{in}$). We operate the detector at -3 dBm, which is in the peak-detection region. This operating mode is safe for regular AN measurement, but it would not be suitable for other applications requiring true quadratic detection, such as beating two RF tones.

The system needs adjustment and calibration. We first set η and θ to the desired value by adjusting phase and amplitude of V_1 and V_2. With reference to Fig. 6, we start with V_1 and V_2 just below the full-scale range. In this condition, $V_1 - V_2$ is determined by the arbitrary phase difference plus the small amplitude asymmetry. Then, we adjust phase and amplitude alternatively for maximum carrier suppression by monitoring

Fig. 5. Experimental setup.

TABLE II
OPERATING PARAMETERS OF FIG. 5

η	V_Δ	V_M	Gain	V_{in}	V_D	V_{DC}
-20	-22	-26	40	$+10$	-3	86
-30	-32	-36	40	0	-3	86
-40	-42	-46	60	$+10$	-3	86
-49	-51	-55	60	$+1$	-2	86
dB	dBm	dBm	dB	dBm	dBm	mV
'V' given in dBm stands for 'the power of the signal V.' For reference, 0 dBm on 50 Ω is 224 mV_{rms}.						

Fig. 6.   Adjustment procedure. (a) Full carrier suppression. (b) Add a small carrier.

the residual carrier. The monitor is an oscilloscope triggered by the 125-MHz reference at one output of the AD9144 or a spectrum analyzer. The spectrum analyzer is easier to use, but the oscilloscope gives access to the sign of the error signal. Manually adjusting phase and amplitude for maximum carrier rejection, we found that the binary search suffers from convergence instability due to uncertainty and fluctuations. This problem is solved by using a subbinary search, which is a binary-like search with smaller steps. Of course, it takes a larger number of iterations. After the maximum carrier

rejection, we set the desired amount of residual carrier by changing V_2. We recommend to check on AM–PM gain and crosstalk by adding a digital modulation to the DAC under test.

IV. RESULTS

Fig. 7 shows the PM and AM noises of the AD9144 measured with different gain levels. All the spectra in this section refer to the total noise of the two output channels; hence, the noise of one channel is 3 dB lower.

In the first experiment [see Fig. 7(a) and (b)], we use the PN analyzer to measure both the PM and AM noises. Fig. 7(a) shows the raw PN spectra as displayed by the PN analyzer, for different values of the gain $1/\eta$ from 20 to 49 dB. Fig. 7(b) reports the same spectra, corrected for the gain. The plots overlap perfectly on almost all the frequency span, indicating that the value of $1/\eta$ is not critical. In the upper half-decade, the noise is some 1 dB higher at lower gain. We did not investigate further on this small discrepancy. Likewise, Fig. 7(c) and (d) shows the AM noise measured with the PN analyzer. The residual carrier is orthogonal to the input carrier ($\theta = \pi/2$) so that the system performs AM-to-PM conversion. The raw spectra [see Fig. 7(c)] are correctly given in rad^2/Hz, as displayed by the PN analyzer. The same spectra, corrected for the gain, are shown in Fig. 7(d). This is the AM noise of the two channels of the AD9144. The unit is dB/Hz, as appropriate. As before, the results overlap on almost the full span but for a small discrepancy in the upper half-decade. Here, the noise measured with the lower gain (20 dB) is some 1.5 dB higher. The bump at 100 kHz, 5 dB above the asymptotic approximation, is probably due to the power supply. We exclude the AD9144 internal reference because it is a common-mode signal and has at most a second-order effect on the AN.

In the second experiment, we measure AN and PN using the AN detector [see Fig. 7(e) and (f)]. The maximum frequency is limited by the full span of the FFT analyzer, which is

Fig. 7. PN and AN of the AD9144, two channels. The four options are shown, with modulation-index amplification and AM–PM cross amplification, and the two types of detection, AM and PM. (a) PN measured with PN analyzer, raw spectra. (b) PN measured with PN analyzer. (c) AN measured with PN analyzer, raw spectra. (d) AN measured with PN analyzer. (e) AN measured with AN analyzer. (f) PN measured with AN analyzer. The spectra in (b) are the same of (a), but in (b), we account for the gain, likewise, in (d) and (c).

of 100 kHz. The AM noise spectra overlap well on most of the span [see Fig. 7(e)]. A small spread, ± 1 dB, shows up in the upper decade. The almost-flat region beyond 10 kHz is actually the bump already seen in the AM noise spectra [see Fig. 7(d)]. The PM noise spectra [see Fig. 7(f)] overlap well with a maximum spread of ± 1.5 dB in the upper decade. In both cases, the higher noise is observed with the lowest gain, 20 dB. This is ascribed to the background noise of the AM detector, which cannot be rejected.

Because a white floor is not visible in any plot shown in Fig. 7, we can only evaluate the upper bound and check on the consistency with the design parameters. From the value $S_\alpha = -161$ dB/Hz based on the data sheet and accounting for 1-dB contribution of the RF amplifier, we expect $S_\alpha = -160$ dB/Hz for the two converters. This is exactly equal to the lowest value seen in Fig. 7(d) (40- and 49-dB/rad gain) at $f = 850$ kHz. Inspecting on S_φ, the lowest value seen in Fig. 7(d) (40- and 49-dB/radgain) is of -159 dB/Hz at $f = 850$ kHz, that is, 1 dB higher than the AN. This indicates that the measured values are consistent with the design.

Fig. 8 compares the above-mentioned results with 30-dB gain. The two AM noise spectra overlap, and likewise the two PM noise spectra. This confirms that the two variants of the method, AN analyzer and PN analyzer, give equivalent results.

The flicker of amplitude is $h_{-1} = 8 \times 10^{-12}$ (-110 dB/Hz at 1 Hz) up to a few kHz, corrupted by a bump at 100 kHz. Such flicker is equivalent to a fractional amplitude stability $\sigma_\alpha = 3.3 \times 10^{-6}$ (Allan deviation). This is found using the classical formula $\sigma^2 = 2\ln(2)\,h_{-1}$, which holds for flicker [23], [43].
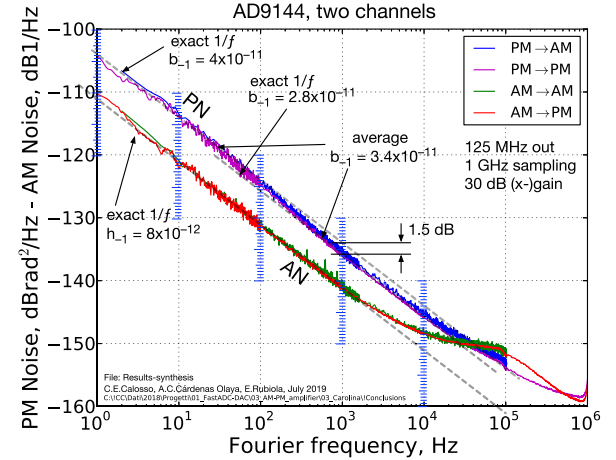
Fig. 8. Comparison of the results with 30-dB gain. The full span of the FFT analyzer limits the AM $\rightarrow$ AM and PM $\rightarrow$ AM spectra to 100 kHz.

The flicker of phase takes two levels: $b_{-1} = 4 \times 10^{-11}$ rad^2 (-104 dBrad^2) at lower f and $b_{-1} = 2.8 \times 10^{-11}$ (-105.5 dBrad^2) at higher f, with a discrepancy of 1.5 dB. The average of these two values is $b_1 = 3.4 \times 10^{-11}$ rad^2. The latter, converted into time-fluctuation PSD, is $S_x = k_{-1}/f$ with $k_{-1} = 5.5 \times 10^{-29}$ s^2. Using $\sigma^2 = 2\ln(2)\,k_{-1}$, we find a time fluctuation $\sigma_x = 8.7$ fs. This value is a combination of *time-type noise* (σ_x is independent of the carrier frequency ν) and the *phase-type noise* [$S_\varphi(f)$ is independent of ν, and σ_x scales as $1/\nu$]. The definitions and the properties of these types of noise are detailed in [43]. Determining the amount
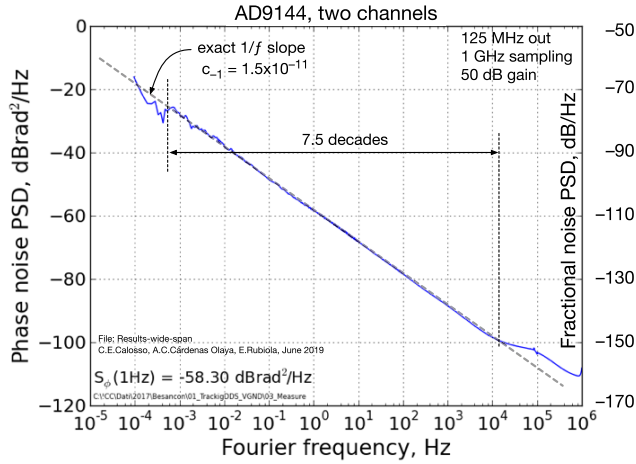
Fig. 9. Flicker noise observed on the widest span. Because θ is not calibrated, the measured quantity (right-hand scale) is a combination of AM and PM.

of phase-type noise and time-type noise requires testing at multiple frequencies, which we have still not done.

Fig. 9 shows the $1/f$ noise measured on the widest span. The experiment was done in Besançon with the alternate configuration mentioned. The calibration is unfortunately less reliable than in the other cases. The gain is of 50 dB, but the phase of the residual carrier was not correctly set. Thus, we assessed θ *a posteriori* using the flicker coefficients of

$$S_\psi = \frac{1}{\eta^2}[\sin^2(\theta)\, S_\alpha + \cos^2(\theta)\, S_\varphi]. \tag{27}$$

The observed quantity is $\eta^2 S_\psi = \mathsf{c}_{-1}/f$ with $\mathsf{c}_{-1} = 1.5 \times 10^{-11}$ (from Fig. 9), and the reference quantities are $\mathsf{h}_{-1} = 8 \times 10^{-12}$ and $\mathsf{b}_{-1} = 3.4 \times 10^{-11}$ (average of the two levels shown), found in Fig. 8. Solving

$$\mathsf{c}_1 = \mathsf{h}_{-1}[1 - \cos(2\theta)] + \mathsf{b}_{-1}\cos^2(\theta) \tag{28}$$

we find $\cos^2(\theta) = 0.26$, and finally, $\theta = 1.03$ rad (59°). Accordingly, the observed result is

$$\eta^2 S_\psi = [0.74\, S_\alpha + 0.26\, S_\varphi]. \tag{29}$$

Regardless of the accuracy of θ, the relevance of this result is the observation of the flicker noise with exact $1/f$ slope over 7.5 decades with a maximum discrepancy of 1 dB.

V. Conclusion

We have proposed a method for the measurement of PM and AM noises of DACs and DDSs, and we have proved the concept by measuring an AD9144.

The value of the method is in its reliability and simplicity. Implementation and use require modest skill in analog RF electronics and only standard skill in programming and using the target DACs and DDSs. Our experiments rely on commercial parts only, such as the Z-Board and DAC daughterboards, and on ready-to-use connectorized RF modules. Under no circumstance, we had to design and implement ad hoc electronics. The low background noise is inherent in the principle and easy to achieve. The cross spectrum comes, optionally, only after the modulation-index amplification. Consequently, none of the known flaws of the cross spectrum can threat the

reliability of the result. Tuning and calibration can be automated because it is done entirely by setting integer numbers in the target converter. Owing to all these characteristics, our method has the potential to become the standard method for the measurement of AM and PM noises of DACs and DDSs.

The experimentalist has two options, using a dedicated PN analyzer or a simple power detector and a general-purpose FFT analyzer. Complexity and background noise are equivalent, and the results overlap.

The power-detector option does not require a PN analyzer, which is a specialized and expensive instrument. The FFT analyzer can be implemented in GNU radio on the Z-Board, after adding an ADC daughterboard. Overall, this version probably fits in the budget of a radio amateur or hobbyist.

The other option requires a commercial PN analyzer. In fact, the design and implementation of such an instrument is definitely not simple. The virtue of a fully digital PN is the wide dynamic range, inherent in the CORDIC algorithm used to extract the random phase modulation from the sampled input [44].

As a fringe benefit, we observed the noise of the AD9144 on a frequency span of ten decades. The flicker noise matches the exact $1/f$ law with a maximum discrepancy of ± 1 dB over 7.5 decades. The flicker noise of an electronic device over such a wide frequency range has probably never been reported before.

References

[1] W. Kester, Ed., *Analog-Digital Conversion*. Norwood, MA, USA: Analog Devices, 2004.

[2] B. Murmann, "The race for the extra decibel: A brief review of current ADC performance trajectories," *IEEE Solid-State Circuits Mag.*, vol. 7, no. 3, pp. 58–66, Summer 2015.

[3] T. Neu, "Clocking the RF ADC with phase noise instead of jitter," *Microw. J.*, vol. 60, no. 8, pp. 100–106, Aug. 2017.

[4] L. Cordesses, "Direct digital synthesis: A tool for periodic wave generation (part 1)," *IEEE Signal Process. Mag.*, vol. 21, no. 4, pp. 50–54, Jul. 2004.

[5] L. Cordesses, "Direct digital synthesis: A tool for periodic wave generation (part 2)," *IEEE Signal Process. Mag.*, vol. 21, no. 5, pp. 110–112, Sep. 2004.

[6] M. Verhelst and A. Bahai, "Where analog meets digital: Analog-to-information conversion and beyond," *IEEE Solid-State Circuits Mag.*, vol. 7, no. 3, pp. 67–80, Jun. 2015.

[7] R. Winoto, "Digital radio-frequency transmitters: An introduction and tutorial," *IEEE Solid-State Circuits Mag.*, vol. 10, no. 4, pp. 70–80, Fall 2018.

[8] M. Clara, *High-Performance D/A-Converters: Application to Digital Transceivers*. New York, NY, USA: Springer, 2013.

[9] P. Harpe, A. Baschirotto, and K. A. A. Makinwa, *High-Performance AD and DA Converters, IC Design in Scaled Technologies, and Time-Domain Signal Processing*. Cham, Switzerland: Springer, 2015.

[10] B. Hoefflinger, Ed., *CHIPS 2020: New Vistas in Nanoelectronics*, vol. 2. Cham, Switzerland: Springer, 2016,

[11] G. Manganaro, *Advanced Data Converters*. Cambridge, U.K.: Cambridge Univ. Press, 2012.

[12] G. Manganaro and D. M. W. Leenaerts, Eds., *Advances in Analog and RF IC Design for Wireless Communication Systems*. Oxford, U.K.: Academic, 2013.

[13] P. Symons, *Digital Waveform Generation*. New York, NY, USA: Cambridge Univ. Press, 2013.

[14] C. A. Ryan, B. R. Johnson, D. Ristè, B. Donovan, and T. A. Ohki, "Hardware for dynamic quantum computing," *Rev. Sci. Instrum.*, vol. 88, no. 10, Oct. 2017, Art. no. 104703.

[15] E. Perego, M. Pomponio, A. Detti, L. Duca, C. Sias, and C. E. Calosso, "A scalable hardware and software control apparatus for experiments with hybrid quantum systems," *Rev. Sci. Instrum.*, vol. 89, no. 11, Oct. 2018, Art. no. 113116.

[16] B. François, C. E. Calosso, M. A. Hafiz, S. Micalizio, and R. Boudot, "Simple-design ultra-low phase noise microwave frequency synthesizers for high-performing Cs and Rb vapor-cell atomic clocks," *Rev. Sci. Instrum.*, vol. 86, no. 9, 2015, Art. no. 094707.

[17] K. Predehl *et al.*, "A 920-kilometer optical fiber link for frequency metrology at the 19th decimal place," *Science*, vol. 336, no. 6080, pp. 441–444, 2012.

[18] D. Calonico *et al.*, "High-accuracy coherent optical frequency transfer over a doubled 642-km fiber link," *Appl. Phys. B*, vol. 117, no. 3, pp. 979–986, Dec. 2014.

[19] O. Lopez, A. Haboucha, B. Chanteau, C. Chardonnet, A. Amy-Klein, and G. Santarelli, "Ultra-stable long distance optical frequency distribution using the Internet fiber network," *Opt. Express*, vol. 20, no. 21, pp. 23518–23526, Oct. 2012.

[20] C. E. Calosso, "Tracking DDS in time and frequency metrology," in *Proc. Joint Eur. Freq. Time Forum Int. Freq. Control Symp. (EFTF/IFCS)*, Prague, Czech Republic, Jul. 2013, pp. 747–749.

[21] *Conferences and Meetings on Particle Accelerators*. Accessed: Jun. 7, 2019. [Online]. Available: https://www.conference-service.com/conferences/particle-accelerators.html

[22] P. Delos and J. Liner, "Improved DAC phase noise measurements enable ultralow phase noise DDS applications," *Analog Dialogue*, vol. 51, no. 3, pp. 31–35, Aug. 2017.

[23] *IEEE Standard Definitions of Physical Quantities for Fundamental Frequency and Time Metrology—Random Instabilities*, IEEE Standard 1139-2008, Feb. 2009, pp. c1–35. doi: 10.1109/IEEESTD.2008.4797525.

[24] J. Rutman and F. L. Walls, "Characterization of frequency stability in precision frequency sources," *Proc. IEEE*, vol. 79, no. 7, pp. 952–960, Jul. 1991.

[25] J. Rutman, "Characterization of phase and frequency instabilities in precision frequency sources: Fifteen years of progress," *Proc. IEEE*, vol. 66, no. 9, pp. 1048–1075, Sep. 1978.

[26] E. Rubiola, "The measurement of AM noise of oscillators," Dec. 2005, *arXiv:0512082*. [Online]. Available: https://arxiv.org/abs/physics/0512082#

[27] C. E. Calosso, Y. Gruson, and E. Rubiola, "Phase noise in DDS," in *Proc. Int. Freq. Control Symp.*, Baltimore, MD, USA, May 2012, pp. 1–6.

[28] J. Grove, J. Hein, J. Retta, P. Schweiger, W. Solbrig, and S. R. Stein, "Direct-digital phase-noise measurement," in *Proc. Int. Freq. Control Symp.*, Montreal, QC, Canada, Aug. 2004, pp. 287–291.

[29] *Phase Noise and Allen Deviation Testers*. Accessed: Jun. 2018. [Online]. Available: https://www.microsemi.com/product-directory/clocks-frequency-references/3834-test-measurement

[30] (2019). *PhaseStation Signal Source Analyzer*. [Online]. Available: http://www.jackson-labs.com/index.php/products/phasestation_signal_source_analyzer

[31] *R&S FSWP Phase Noise Analyzer and VCO Tester*. Accessed: Sep. 20, 2019. [Online]. Available: https://www.rohde-schwarz.com/ca/product/fswp-productstartpage_63493-120512.html

[32] G. Feldhaus and A. Roth, "A 1 MHz to 50 GHz direct down-conversion phase noise analyzer with cross-correlation," in *Proc. Eur. Freq. Time Forum*, York, U.K., Apr. 2016, pp. 1–4.

[33] C. W. Nelson, A. Hati, and D. A. Howe, "A collapse of the cross-spectral function in phase noise metrology," *Rev. Sci. Instrum.*, vol. 85, no. 3, pp. 024705-1–024705-7, Feb. 2014.

[34] Y. Gruson, V. Giordano, U. L. Rohde, A. K. Poddar, and E. Rubiola, "Cross-spectrum PM noise measurement, thermal energy, and metamaterial filters," *IEEE Trans. Ultrason., Ferroelectr., Freq. Control*, vol. 64, no. 3, pp. 634–642, Mar. 2017.

[35] E. Rubiola and F. Vernotte, "The cross-spectrum experimental method," Apr. 2010, *arXiv:1003.0113*. [Online]. Available: https://arxiv.org/abs/1003.0113

[36] K. H. Sann, "The measurement of near-carrier noise in microwave amplifiers," *IEEE Trans. Microw. Theory Techn.*, vol. 16, no. 9, pp. 761–766, Sep. 1968.

[37] F. Labaar, "New discriminator boosts phase-noise testing," *Microwaves*, vol. 21, no. 3, pp. 65–69, Jan. 1982.

[38] E. N. Ivanov, M. E. Tobar, and R. A. Woode, "Microwave interferometry: Application to precision measurements and noise reduction techniques," *IEEE Trans. Ultrason., Ferroelectr., Freq. Control*, vol. 45, no. 6, pp. 1526–1536, Nov. 1998.

[39] E. Rubiola, V. Giordano, and J. Groslambert, "Very high frequency and microwave interferometric phase and amplitude noise measurements," *Rev. Sci. Instrum.*, vol. 70, no. 1, pp. 220–225, Jan. 1999.

[40] F. L. Walls, "Suppressed carrier based PM and AM noise measurement techniques," in *Proc. Int. Freq. Control Symp.*, Orlando, FL, USA, May 1997, pp. 485–492.

[41] R. Boudot and E. Rubiola, "Phase noise in RF and microwave amplifiers," *IEEE Trans. Ultrason., Ferroelectr., Freq. Control*, vol. 59, no. 12, pp. 2613–2624, Dec. 2012.

[42] *AD9144-FMC-EBZ Evaluation Board*. Accessed: Jun. 7, 2019. [Online]. Available: https://wiki.analog.com/resources/eval/dpg/ad9144-fmc-ebz

[43] C. E. Calosso and E. Rubiola, "Phase noise and jitter in digital electronics," Dec. 2016, *arXiv:1701.00094*. [Online]. Available: https://arxiv.org/abs/1701.00094

[44] P. K. Meher, J. Valls, T.-B. Juang, K. Sridharan, and K. Maharatna, "50 years of CORDIC: Algorithms, architectures, and applications," *IEEE Trans. Circuits Syst. I, Reg. Papers*, vol. 56, no. 9, pp. 1893–1907, Sep. 2009.